Abelian Multi-Cycle Codes for Single-Shot Error Correction

Hsiang-Ku Lin,[1] Pak Kau Lim,[1] Alexey A. Kovalev,[2] and Leonid P. Pryadko[3,1,*]

[1] *Department of Physics & Astronomy, University of California, Riverside, California 92521, USA*

[2] *Department of Physics and Astronomy and Nebraska Center for Materials and Nanoscience, University of Nebraska, Lincoln, Nebraska 68588, USA*

[3] *Google Quantum AI, Santa Barbara, California 93117, USA*

(Received 26 August 2025; revised 11 December 2025; accepted 23 March 2026; published 11 May 2026)

We construct a family of quantum low-density parity-check codes locally equivalent to higher-dimensional quantum hypergraph-product (QHP) codes. Similarly to QHP codes, the proposed codes have highly redundant sets of low-weight stabilizer generators, which improves decoding accuracy in a fault-tolerant regime and gives them single-shot properties. The advantage of the construction is that it gives shorter codes. We derive simple expressions for the dimension of the proposed codes in two important special cases, give bounds on the distances and explicitly construct some relatively short codes. Circuit simulations for codes locally equivalent to four-dimensional toric codes show a (pseudo)threshold close to 1.1%, better than for toric or surface codes with a similar noise model.

DOI: 10.1103/mj28-925w

I. INTRODUCTION.

Quantum error correction (QEC) is one of the key enabling technologies for scalable quantum computation. Despite a lot of effort in the community, it took over a quarter century after discovery of QEC [1,2] for quantum memory experiments based on surface codes [3–5] to demonstrate logical error rates that are well in the scalable regime [6–9]. A major difficulty here is the need to operate fault-tolerantly, in the presence of errors that occur during the syndrome measurement.

A general approach to fault-tolerance (FT) is to use redundant syndrome measurements. For quantum memory and logical Clifford gates, the redundancy can be gained from repeated measurements, as it is sufficient to track just the Pauli basis associated with the current error. The resulting classical syndrome-based decoding problem can be solved sequentially, using measured syndrome data from a few cycles at a time [5,10]. On the other hand, non-Clifford gates needed for universal quantum computation require real-time decoding. Even though some delay can be tolerated at the cost of increased circuit complexity, shorter lag times are strongly preferable [11]. From this viewpoint, optimal is single-shot decoding [12–14], where syndrome data from each measurement cycle are processed right after it becomes available.

Single-shot fault-tolerant QEC requires measuring some redundant stabilizer generators. This redundancy helps to control measurement errors and thus enables independent decoding of each batch of syndrome data. Such ideas go back to the seminal work [5] of Dennis *et al.*; various coding theory aspects have been studied in, e.g., Refs. [15–17]. Single-shot properties have been studied numerically and analytically for a number of code families, including higher-dimensional hyperbolic codes [18], as well as higher-dimensional toric [19], and more general quantum hypergraph-product (QHP) codes [20–23].

Unfortunately, the product constructions tend to give rather long codes. Recently, the effect of natural redundancy in two-block and generalized-bicycle (GB) codes [24] with stabilizer generators of weight six has been studied by three of the present authors [25]. These, and more general 2BGA codes [26–28], including the bivariate-bicycle (BB) codes [29–32], have attracted attention as the family which contains short codes with relatively high rates and distances (substantially improving over the surface/toric codes) and at the same time with relatively high thresholds. While GB codes constructed in Ref. [25] saturate an upper bound on the syndrome distance, their single-shot properties turned out to be limited by the lack of confinement.

More recently, Aasen *et al.* proposed a family of four-dimensional geometric toric codes [33,34] locally equivalent to 4D toric codes, but on a 4-torus with periodicity vectors not necessarily along the principal lattice

*Contact author: pryadko@google.com

Published by the American Physical Society under the terms of the Creative Commons Attribution 4.0 International license. Further distribution of this work must maintain attribution to the author(s) and the published article's title, journal citation, and DOI.

directions. They analyzed the performance of the constructed codes in circuit simulations of quantum memory experiments and studied their single-shot properties. They also designed a number of protected operations on logical qubits, including state injection and the unitaries generating the entire Clifford group on the logical qubits.

In this work we construct a family of multiblock chain (MBC) complexes, and their implementation using abelian group algebra matrices, which we call abelian multicycle (AMC) codes. This construction is strictly more general than 4D geometric toric codes in Refs. [33,34], in the sense that all their codes are included in our construction. Our MBC codes are related to higher-dimensional QHP codes [20,21] in exactly the same way as two-block codes are related to the original (two-dimensional) QHP codes [35], and they share many properties with both the two-block codes and higher-dimensional QHP codes. In addition to the general construction, we give analytic expressions for the code dimensions in two important general cases and also give lower (existence) and upper bounds for the distances. As an important example, we study the family of AMC codes locally equivalent to four-dimensional toric codes. All these codes have stabilizer generators of weight 6 and encode $k = 6$ logical qubits. We explicitly construct a number of such codes, calculate their parameters and perform circuit simulations to compute a (pseudo)threshold and analyze the accuracy of few-shot sliding-window (SW) decoding.

II. DEFINITIONS

For a given finite (Galois) field $F \equiv \mathbb{F}_q$, of size $|F| = q = p^m$ and prime characteristic p, an F-linear code of length n and dimension k is a linear space $\mathcal{C} \subseteq F^n$ of dimension k. Any set of $k = \operatorname{rank} G$ linearly independent rows of an F-valued *generator* matrix G with n columns forms a basis of the code $\mathcal{C} \equiv \mathcal{C}_G$ generated by G; this code has length n and dimension k. The dual code $\mathcal{C}^\perp \equiv \mathcal{C}_G^\perp$ of dimension $n-k$ is formed by all vectors in F^n orthogonal to nonzero vectors in $\mathcal{C}$ or, equivalently, to the rows of G, a *check* matrix of the code $\mathcal{C}_G^\perp$.

For a given finite field F and a finite group G of order $|G| = \ell$, the (Hopf) *group algebra* (also, a ring) $F[G]$ is defined as an F-linear space of all formal sums

$$x \equiv \sum_{g\in G} x_g g, \quad x_g \in F, \tag{1}$$

where group elements $g \in G$ serve as basis vectors, equipped with the product naturally associated with the group operation,

$$ab = \sum_{g\in G}\left(\sum_{h\in G} a_h b_{h^{-1}g}\right) g, \quad a, b \in F[G]. \tag{2}$$

Evidently, Eq. (1) defines a one-to-one map between any vector $\boldsymbol{x} \in F^\ell$ with coefficients x_g labeled by group elements and a group algebra element $x \in F[G]$, and a related map between sets of vectors and sets of group algebra elements. In this work we consider only group algebras constructed from abelian groups. An abelian group code in F^ℓ is a map (1) of an ideal J in an abelian ring $F[G]$, defined as an F-linear space of elements of $F[G]$ such that for any $x \in J$ and any $r \in F[G]$, $rx \in J$. An ideal $J \le F[G]$ is called [36] checkable if there is an element $a \in F[G]$ such that $J = \{x | x \in F[G], ax = 0\}$.

A *chain complex* is a sequence of abelian groups and homomorphisms between pairs of consecutive groups such that the image of each homomorphism is included in the kernel of the next. Here we will be concerned with the special case of chain complexes of finite-dimensional vector spaces $\ldots, \mathcal{A}_{j-1}, \mathcal{A}_j, \ldots$ over a finite field F, and we denote the space dimensions $n_j \equiv n_j(\mathcal{A}) = \dim \mathcal{A}_j$. In this case the boundary operators are linear transformations $\partial_j : \mathcal{A}_{j-1} \leftarrow \mathcal{A}_j$ that map between each pair of neighboring spaces, with the requirement $\partial_j \partial_{j+1} = 0, j \in \mathbb{Z}$. We define a D-complex $\mathcal{A} \equiv \mathcal{K}(A_1, \ldots, A_D)$, a bounded chain complex which only contains $D+1$ nontrivial spaces with fixed bases, in terms of $n_{j-1} \times n_j$ matrices A_j over F serving as the boundary operators, $j \in \{1, \ldots, D\}$,

$$\mathcal{A} : \ldots \leftarrow \{0\} \overset{\partial_0}{\leftarrow} \mathcal{A}_0 \overset{A_1}{\leftarrow} \mathcal{A}_1 \ldots \overset{A_D}{\leftarrow} \mathcal{A}_D \overset{\partial_{D+1}}{\leftarrow} \{0\} \ldots \tag{3}$$

Here, the products of neighboring matrices must be zero, $A_{j-1}A_j = 0, j \in \{2, \ldots, D\}$. In addition to boundary operators given by the matrices A_j, implicit are the trivial operators $\partial_0 : \{0\} \leftarrow \mathcal{A}_0$ and $\partial_{D+1} : \mathcal{A}_D \leftarrow \{0\}$ (with the image being the zero vector in $\mathcal{A}_D$) treated formally as rank-zero $0 \times n_0$ and $n_D \times 0$ matrices.

Elements of the subspace $\operatorname{im}(\partial_j) \subseteq \mathcal{A}_{j-1}$ are called boundaries; in our case, these are linear combinations of columns of A_j and, therefore, form an F-linear code with the generator matrix A_j^T, $\operatorname{im}(A_j) = \mathcal{C}_{A_j^T}$. Elements of $\operatorname{Ker}(\partial_j) \subset \mathcal{A}_j$ are called cycles; in our case, these are vectors in an F-linear code with the parity check matrix A_j, $\operatorname{Ker}(A_j) = \mathcal{C}_{A_j}^\perp$.

Because of the orthogonality $\partial_j \partial_{j+1} = 0$, all boundaries are necessarily cycles, $\operatorname{im}(\partial_{j+1}) \subseteq \operatorname{Ker}(\partial_j) \subseteq \mathcal{A}_j$. The structure of the cycles in $\mathcal{A}_j$ that are not boundaries is described by the jth homology group,

$$H_j(\mathcal{A}) \equiv H(A_j, A_{j+1}) = \operatorname{Ker}(A_j)/\operatorname{im}(A_{j+1}). \tag{4}$$

Group quotient here means that two cycles that differ by a boundary are considered equivalent; nonzero elements of $\mathcal{H}_j(\mathcal{A})$ are equivalence classes of homologically nontrivial cycles. Explicitly, the equivalence of $\boldsymbol{x}$ and $\boldsymbol{y}$ in $\mathcal{A}_j$, denoted as $\boldsymbol{x} \simeq \boldsymbol{y}$, implies that for some $\boldsymbol{\alpha} \in \mathcal{A}_{j+1}$, $\boldsymbol{y} = \boldsymbol{x} + \boldsymbol{\alpha} A_{j+1}^T$. The rank of jth homology group is the

dimension of the corresponding vector space; one has

$$k_j \equiv \operatorname{rank} H_j(\mathcal{A}) = n_j - \operatorname{rank} A_j - \operatorname{rank} A_{j+1}. \quad (5)$$

The homological *distance* d_j is the minimum Hamming weight of a nontrivial element (any representative) in the homology group $H_j(\mathcal{A}) \equiv H(A_j, A_{j+1})$,

$$d_j = \min_{\mathbf{0}\neq \boldsymbol{x}\in H_j(\mathcal{A})} \operatorname{wgt} \boldsymbol{x} = \min_{\boldsymbol{x}\in \operatorname{Ker}(A_j)\setminus \operatorname{im}(A_{j+1})} \operatorname{wgt} \boldsymbol{x}. \quad (6)$$

By this definition $d_j \geq 1$. To address singular cases, the minimum of an empty set is defined as infinity; $k_j = 0$ is always equivalent to $d_j = \infty$. In particular, the distance of the homology group $H_0(\mathcal{A})$ is $d_0 = 1$, unless A_1 has full row rank, giving $k_0 = 0$, in which case $d_0 = \infty$. In the case of the homology group $H_D(\mathcal{A})$, the distance d_D is that of the F-linear code with the check matrix A_D.

In addition to the homology group $H(A_j, A_{j+1})$, there is also a *co-homology* group $\tilde{H}_j(\tilde{\mathcal{A}}) = H(A_{j+1}^T, A_j^T)$ of the same rank (5); this is associated with the *co-chain complex* $\tilde{\mathcal{A}}$ formed from the transposed matrices A_j^T taken in the opposite order. A quantum CSS code [37,38] with generator matrices $G_X = A_j$ and $G_Z = A_{j+1}^T$ is isomorphic with the direct sum of the groups H_j and $\tilde{H}_j$,

$$\operatorname{CSS}(A_j, A_{j+1}^T) \cong H(A_j, A_{j+1}) \oplus H(A_{j+1}^T, A_j^T). \quad (7)$$

The two terms correspond to Z and X logical operators, respectively, with stabilizer generator matrices $H_X = A_j$ and $H_Z = A_{j+1}^T$. This gives for the homological distances in the chain complex and in the co-chain complex, respectively, $d_j = d_Z$ and $\tilde{d}_j = d_X$.

Quantum codes operate in a fault-tolerant (FT) regime, where errors may happen during the syndrome measurement. Commonly used in such a situation is the tactic of redundant measurements. Assuming each operator being measured has the corresponding row in H_X or H_Z, redundancy implies the existence of nontrivial matrices M_X and M_Z such that $M_X H_X = 0$, $M_Z H_Z = 0$. Rows of M_X and M_Z, respectively, correspond to X and Z metachecks [14]. Evidently, a quantum CSS code with redundant measurements forms a 4-chain complex with boundary operators M_X, H_X, H_Z^T, M_Z^T. In particular, Campbell *et al.* argued [14,22] that longer complexes constructed as tensor products of 1-complexes have nice error-correction properties in the FT regime and they can be used for single-shot error correction.

Tensor product $\mathcal{A} \times \mathcal{B}$ of two chain complexes $\mathcal{A}$ and $\mathcal{B}$ is defined as the chain complex formed by linear spaces decomposed as direct sums of Kronecker products,

$$(\mathcal{A} \times \mathcal{B})_j = \bigoplus\nolimits_{i\in\mathbb{Z}} \mathcal{A}_i \otimes \mathcal{B}_{j-i}, \quad (8)$$

with the action of the boundary operators

$$\partial'''(\boldsymbol{a} \otimes \boldsymbol{b}) \equiv \partial' \boldsymbol{a} \otimes \boldsymbol{b} + (-1)^i \boldsymbol{a} \otimes \partial'' \boldsymbol{b}, \quad (9)$$

where $\boldsymbol{a} \in \mathcal{A}_i$, $\boldsymbol{b} \in \mathcal{B}_{j-i}$, and the boundary operators ∂', ∂'', and ∂''' act in complexes $\mathcal{A}$, $\mathcal{B}$, and $\mathcal{A} \times \mathcal{B}$, respectively. Notice that the two terms in Eq. (9) are supported in different subspaces of the expansion (8). When both $\mathcal{A}$ and $\mathcal{B}$ are *bounded*, the dimension $n_j(\mathcal{C})$ of a space $\mathcal{C}_j$ in the product $\mathcal{C} = \mathcal{A} \times \mathcal{B}$ is

$$n_j(\mathcal{C}) = \sum\nolimits_i n_i(\mathcal{A})\, n_{j-i}(\mathcal{B}). \quad (10)$$

The homology groups of the product $\mathcal{C} = \mathcal{A} \times \mathcal{B}$ are isomorphic to a simple expansion in terms of those of $\mathcal{A}$ and $\mathcal{B}$ which is given by the Künneth formula,

$$H_j(\mathcal{C}) \cong \bigoplus\nolimits_i H_i(\mathcal{A}) \otimes H_{j-i}(\mathcal{B}). \quad (11)$$

One immediate consequence is that the rank $k_j(\mathcal{C})$ of the j th homology group $H_j(\mathcal{C})$ is

$$k_j(\mathcal{C}) = \sum\nolimits_i k_i(\mathcal{A})\, k_{j-i}(\mathcal{B}). \quad (12)$$

For the homological distances in a product of two arbitrary-length complexes, we have some bounds [21],

$$\min_{i\in\mathbb{Z}} \max\left(d_i(\mathcal{A}), d_{j-i}(\mathcal{B})\right) \leq d_j(\mathcal{C}) \leq \min_{i\in\mathbb{Z}} d_i(\mathcal{A}) d_{j-i}(\mathcal{B}). \quad (13)$$

The exact distances are known only in the important case where one of the factors is a 1-complex [20,21,35]. With a D-complex $\mathcal{A}$ in Eq. (3) and a 1-complex $\mathcal{B} \equiv \mathcal{K}(B_1)$, the homological distances are [21]

$$d_j(\mathcal{C}) = \min\left(d_j(\mathcal{A}) d_0(\mathcal{B}), d_{j-1}(\mathcal{A}) d_1(\mathcal{B})\right). \quad (14)$$

In the following, we refer to a D-fold product of 1-complexes as a D-dimensional QHP complex [20,21,35]. Such a D-complex $\mathcal{Q}$ has $D+1$ nontrivial linear spaces $\mathcal{Q}_j$, with $0 \leq j \leq D$, where the space at level j is formed as a direct sum of $m_j^{(D)}$ product subspaces,

$$\mathcal{A}_{j_1}^{(1)} \times \mathcal{A}_{j_2}^{(2)} \times \cdots \times \mathcal{A}_{j_D}^{(D)}.$$

Here, the level index $j = j_1 + j_2 + \cdots + j_D$ is a sum of individual level indices $j_i \in \{0, 1\}$. The number of such terms is given by a binomial,

$$m_j^{(D)} = \binom{D}{j}. \quad (15)$$

In particular, consider a 1-complex $\mathcal{A} \equiv \mathcal{K}(A)$, where A is a square $n \times n$ matrix such that the F-linear code $\mathcal{C}_A^{\perp}$ has

parameters $[n,k,d]$. Its D-fold tensor product with itself, $\mathcal{Q}=\mathcal{A}^{\times D}$, has space dimensions

$$n_j^{(D)}=\binom{D}{j}n^D,\quad 0\le j\le D, \tag{16}$$

and the dimension and the homological distance of its jth homology group $H_j(\mathcal{Q})$ are, respectively,

$$k_j^{(D)}=\binom{D}{j}k^D,\quad d_j^{(D)}=d^j,\quad 0\le j\le D. \tag{17}$$

III. CONSTRUCTION AND CODE PROPERTIES

A. Multiblock complexes and associated quantum codes

We construct a *multiblock chain* (MBC) complex as a generalization of D-dimensional QHP codes in exactly the same fashion as the two-block codes have been constructed as a generalization of regular (2D) HP codes [24]. The given matrices A_1 and B_1 over F, with dimensions $n_0(\mathcal{A})\times n_1(\mathcal{A})$ and $n_0(\mathcal{B})\times n_1(\mathcal{B})$, respectively, the tensor product $\mathcal{P}=\mathcal{A}\times\mathcal{B}$ of the complexes $\mathcal{A}\equiv\mathcal{K}(A_1)$ and $\mathcal{B}\equiv\mathcal{K}(B_1)$, explicitly,

$$\mathcal{P}:\ldots\{0\}\overset{\partial_0}{\leftarrow}\mathcal{A}_0\times\mathcal{B}_0\overset{P_1}{\leftarrow}\begin{matrix}\mathcal{A}_0\times\mathcal{B}_1\\ \mathcal{A}_1\times\mathcal{B}_0\end{matrix}\overset{P_2}{\leftarrow}\mathcal{A}_1\times\mathcal{B}_1\leftarrow\{0\}\ldots,$$

has the boundary operators [cf. Eq. (9)]

$$P_1=[I_A\otimes B_1, A_1\otimes I_B],\quad P_2=\begin{bmatrix}A_1\otimes I_B\\ -I_A\otimes B_1\end{bmatrix}, \tag{18}$$

where $I_A\equiv I(\mathcal{A}_0)$ and $I_B\equiv I(\mathcal{B}_0)$ are the identity operators on the spaces $\mathcal{A}_0$ and $\mathcal{B}_0$, respectively. The product vanishes, $P_1P_2=0$, because the two blocks, $A\equiv A_1\otimes I_B$ and $B\equiv I_A\otimes B_1$, commute. The generalization [24] is evident: for any pair of $\ell\times\ell$ square commuting matrices, $AB=BA$, the two-block code has the CSS matrices,

$$H_X\equiv P_1=[B,A],\quad H_Z^T\equiv P_2=\begin{bmatrix}A\\ -B\end{bmatrix}. \tag{19}$$

We regard this construction as the smallest (two-dimensional) multiblock chain complex, and denote it $\mathcal{P}=\mathrm{MBC}(A,B)$, with the requirement $AB=BA$.

Similarly, to define a three-dimensional generalization, a *3-chain complex* $\mathrm{MBC}(A,B,C)$ from three pairwise commuting matrices, we insert an additional 1-complex into the product, $\mathcal{Q}\equiv\mathcal{A}\times\mathcal{B}\times\mathcal{C}=\mathcal{P}\times\mathcal{C}$, with the nontrivial subspaces,

$$\mathcal{P}_0\times\mathcal{C}_0\overset{Q_1}{\leftarrow}\begin{matrix}\mathcal{P}_0\times\mathcal{C}_1\\ \mathcal{P}_1\times\mathcal{C}_0\end{matrix}\overset{Q_2}{\leftarrow}\begin{matrix}\mathcal{P}_1\times\mathcal{C}_1\\ \mathcal{P}_2\times\mathcal{C}_0\end{matrix}\overset{Q_3}{\leftarrow}\mathcal{P}_2\times\mathcal{C}_1.$$

The subspaces in direct sums are stacked vertically [cf. Eq. (8)] and ordered alphabetically by the space indices. The structure of the corresponding boundary operators follows directly from the subspace decomposition and the sign convention (9), $Q_1=[I\otimes C_1, P_1\otimes I]$,

$$Q_2=\begin{bmatrix}P_1\otimes I & 0\\ -I\otimes C_1 & P_2\otimes I\end{bmatrix}\text{ and }Q_3=\begin{bmatrix}P_2\otimes I\\ I\otimes C_1\end{bmatrix}.$$

With Eq. (18), it is easy to verify that the resulting matrices contain only three blocks, $A\equiv A_1\otimes I_B\otimes I_C$, $B\equiv I_A\otimes B_1\otimes I_C$, and $C\equiv I_A\otimes I_B\otimes C_1$, and can be explicitly written as

$$Q_1=[C\,|\,B\,A], \tag{20}$$

$$Q_2=\left[\begin{array}{cc|c}B & A & 0\\ -C & 0 & A\\ \hline 0 & -C & -B\end{array}\right], \tag{21}$$

$$Q_3=\left[\begin{array}{c}A\\ -B\\ \hline C\end{array}\right]. \tag{22}$$

We used the lines here to emphasize the inherited block structure, cf. matrices in Eq. (19). Just like for the case of two-block codes, the orthogonality can be verified directly, $Q_1Q_2=0$, $Q_2Q_3=0$, as long as the individual blocks A, B, and C commute.

For a general definition, consider a D-complex $\mathcal{Q}\equiv\mathrm{MBC}(A_1,A_2,\ldots,A_D)$ constructed from D commuting square blocks A_i, $\ell\times\ell$ matrices over F, with boundary operators $\partial_j^{(Q)}=Q_j$, where $Q_jQ_{j+1}=0$. Explicitly, the space dimensions (nonzero for $0\le j\le D$) are $\dim(\mathcal{Q}_j)\equiv n_j^{(Q)}=\binom{D}{j}\ell$; it is also convenient to define the block dimensions $m_j\equiv m_j^{(Q)}=\binom{D}{j}$ such that $n_j=m_j\ell$. Then, given an additional block $A_{D+1}\equiv N$ commuting with those already present, the $(D+1)$-dimensional chain complex $\mathcal{R}\equiv\mathrm{MBC}(A_1,A_2,\ldots,A_D,N)$ has the block dimensions $m_j^{(R)}=m_{j-1}^{(Q)}+m_j^{(Q)}=\binom{D+1}{j}$, and the boundary operators constructed as block matrices,

$$R_1=\begin{bmatrix}N, & Q_1\end{bmatrix}, \tag{23}$$

$$R_i=\begin{bmatrix}Q_{i-1}, & 0\\ (-1)^{i-1}I(m_{i-1})\otimes N, & Q_i\end{bmatrix},\ 1<i\le D, \tag{24}$$

$$R_{D+1}=\begin{bmatrix}Q_D\\ (-1)^D N\end{bmatrix}, \tag{25}$$

where $I(m)$ is an $m\times m$ identity matrix.

For a D-dimensional MBC complex with boundary matrices Q_j, $1 \le j \le D$, it is easy to verify that all D blocks are used in an equivalent fashion, i.e., all chain complexes constructed from the same D commuting blocks taken in different orders are equivalent (can be obtained from each other by block row and column permutations). In particular, matrix Q_j has j nonzero blocks in each column and $D+1-j$ nonzero blocks in each row. Furthermore, in each pair of matrices Q_j and Q_{j+1}^T with $m_j = \binom{D}{j}$ being column blocks, $1 \le j < D$, each pair of matching column-blocks contains a full set of blocks $\{A_i\}$, exactly j such blocks in Q_j and the remaining $D-j$ (transposed) blocks in Q_{j+1}^T.

For future reference, the boundary operators in the 4-complex $\mathcal{R} \equiv \mathrm{MBC}(A,B,C,D)$ are

$$R_1 = [D \,|\, C\,B\,A], \tag{26}$$

$$R_2 = \left[\begin{array}{ccc|ccc} C & B & A & & & \\ \hline -D & & & B & A & 0 \\ & -D & & -C & 0 & A \\ & & -D & 0 & -C & -B \end{array}\right], \tag{27}$$

$$R_3 = \left[\begin{array}{ccc|c} B & A & 0 & \\ -C & 0 & A & \\ 0 & -C & -B & \\ \hline D & & & A \\ & D & & -B \\ & & D & C \end{array}\right], \tag{28}$$

$$R_4 = \left[\begin{array}{c} A \\ -B \\ C \\ \hline -D \end{array}\right]. \tag{29}$$

While any nontrivial homology group in this complex may be used to construct a quantum code, we will focus on $H_2(\mathcal{R}) = H(R_2, R_3)$ and the corresponding co-homology group $\tilde{H}_2(\mathcal{R})$. This gives a self-dual CSS code with generator matrices $H_X = R_2$, $H_Z = R_3^T$.

B. AMC codes

AMC complexes (and associated *quasi-abelian* quantum CSS codes) are a special case of multiblock codes where the commuting matrices are constructed [39] with the help of an abelian group algebra $F[G]$, see Eq. (1). Namely, assuming the group size is $\ell \equiv |G|$, for an element $a \in F[G]$, the $\ell \times \ell$ matrix $A \equiv \mathrm{M}(a)$ is defined by the action of a on the group elements,

$$[\mathrm{M}(a)]_{\alpha,\beta} \equiv \sum_{g\in G} a_g \delta_{\alpha,g\beta}, \tag{30}$$

where group elements $\alpha, \beta \in G$ are used to index rows and columns, and $\delta_{\alpha,\beta} = 1$ if $\alpha = \beta$ and 0 otherwise is the Kronecker delta. It is easy to verify that for group elements $g \in G$, $\mathrm{M}(g)$ are permutation matrices forming the regular F-linear representation of G. Also, since transposition gives the inverse of a permutation matrix, for any $a \in F[G]$, a transposed matrix $[M(a)]^T$ can be obtained from the group algebra element [36],

$$\widehat{a} \equiv \sum_{g\in G} a_{g^{-1}} g = \sum_{g\in G} a_g g^{-1}, \quad [M(a)]^T = M(\widehat{a}). \tag{31}$$

Then, given a sequence $\{a_j\}_{j=1}^D \subset F[G]$ of abelian group algebra elements, with $D \ge 2$, the corresponding matrices $A_j = \mathrm{M}(a_j)$ commute, and the D-complex $\mathcal{Q} \equiv \mathcal{Q}^{(D)} = \mathrm{MBC}(A_1, A_2, \ldots, A_D)$ can be constructed as explained in the previous section. We denote such a D-complex $\mathcal{Q} = \mathrm{AMC}(a_1, a_2, \ldots, a_D)$. The corresponding level-j quantum CSS code $\mathrm{AMC}_j(a_1, a_2, \ldots, a_D)$, $j \le D$, is constructed from the level-j homology $H_j(\mathcal{Q})$ and co-homology $\tilde{H}_j(\mathcal{Q})$ groups. Explicitly,

$$\mathrm{AMC}_j(a_1, a_2, \ldots, a_D) = \mathrm{CSS}(Q_j, Q_{j+1}^T),$$

where Q_j is the jth boundary operator (matrix) in the D-complex $\mathcal{Q}$.

To visualize, consider a finite abelian group

$$G = \langle x_1, x_2, \ldots, x_m | r_1(\boldsymbol{x}), r_2(\boldsymbol{x}), \ldots, r_m(\boldsymbol{x}) \rangle_{\text{abelian}},$$

presented with m commuting generators $x_1, x_2, \ldots, x_m$, and m additional independent (monomial) relators,

$$1_G = r_i(\boldsymbol{x}) = \prod_{j=1}^{m} x_j^{\Delta_j}, \quad \Delta_j \equiv \Delta_j^{(i)}, \quad i = 1, 2, \ldots, m.$$

Further, elements of the free abelian group $\langle x_1, x_2, \ldots, x_m \rangle$ are in a one-to-one correspondence with points of $\mathbb{Z}^m$. The exponents in each relator $r_i(\boldsymbol{x})$ form a basis vector $\boldsymbol{\Delta}^{(i)} = (\Delta_1^{(i)}, \Delta_2^{(i)}, \ldots, \Delta_m^{(i)})$ of a lattice on $\mathbb{Z}^m$; individual basis vectors are combined as columns of a lattice basis matrix Δ. Any two points on $\mathbb{Z}^m$ connected by a lattice vector are identified. Then, elements of the group G are in a one-to-one correspondence with inequivalent points in $\mathbb{Z}^m$ which form an m-torus $\mathcal{T}_m$. The number of inequivalent points (also, the number of points in a primitive cell of the lattice) is $n = |G| = |\det \Delta|$. In the absence of single-variable degree-two relators, the torus $\mathcal{T}_m$ is covered by $\mathbb{Z}^m$, with a well-defined covering function $f : \mathbb{Z}^m \to \mathcal{T}_m$ which is one-to-one in each ball of some radius $r_{\text{inj}} > 0$ on $\mathbb{Z}^m$, the injectivity radius.

The support of an m-variate polynomial over F corresponds to a set of points on $\mathbb{Z}^m$; multiplication by a generator x_j gives a translation along the j-axis. Respectively, the support of a group algebra element $a \equiv a(\boldsymbol{x})$ corresponds to a set of points on the torus $\mathcal{T}_m$.

A group presentation where each relator depends only on the corresponding variable, $r_i = x_i^{\Delta_i}$, with the lattice basis matrix $\Delta = \mathrm{diag}(\Delta_1, \Delta_2, \ldots, \Delta_m)$, corresponds to a decomposition [40] of the finite abelian group as a direct product of cyclic groups,

$$G = C_{\Delta_1} \times C_{\Delta_2} \times \ldots \times C_{\Delta_m}.$$

In such a case, we get a torus with periodicity vectors along the Cartesian axes, and the group order is given by a product, $|G| = \prod_{i=1}^{m} \Delta_i$.

We note that the number of generators in a presentation of the same group may vary. In particular, while any cyclic group $C_n = \langle x | x^n \rangle$ has a single-generator presentation, presentations with two or more variables can always be constructed for a sufficiently large group. For example,

$$C_{15} = C_3 \times C_5 = \langle x, y | x^3, y^5 \rangle_{\text{abelian}}, \quad \Delta = \begin{pmatrix} 3, & 0 \\ 0, & 5 \end{pmatrix},$$

$$C_{15} = \langle x, y | x^4 y, x y^4 \rangle_{\text{abelian}}, \quad \Delta = \begin{pmatrix} 4, & 1 \\ 1, & 4 \end{pmatrix}.$$

where the only condition is that the determinant of the matrix Δ matches the group order, $n = |\det \Delta|$.

C. Equivalent AMC codes

Changing a group presentation, one can try to come up with an equivalent complex, e.g., with better locality properties. How much freedom do we have? To answer this question, let us first discuss the symmetries of AMC construction. The following statement is given without a proof, as a generalization of Theorem 3 in Ref. [28]:

Statement 1. For any sequence $\{a_j\} \equiv \{a_j\}_{j=1}^{D} \subset F[G]$, the D-complex $\mathrm{AMC}(\{a_j\})$ is permutation-equivalent to the D-complex constructed from the modified sequence:

(i) A permuted sequence of group algebra elements;
(ii) $\{\varphi(a_j)\}$, for any automorphism $\varphi : G \to G$;
(iii) $\{x_j a_j\}$, for any nonzero $x_j \in F$;
(iv) $\{a_j \alpha_j\}$, for any $\alpha_j \in G$.

In addition, the sequence $\{\widehat{a}_j\}$, see Eq. (31), gives an AMC complex isomorphic to the original co-chain complex, $\mathrm{AMC}(\{\widehat{a}_j\}) \simeq \widetilde{\mathrm{AMC}}(\{a_j\})$.

Therefore, we can always "rescale" the elements in the original set, and choose $a_j = 1 + \cdots$, $j \le D$. Further, we can try to simplify the polynomials for a D-dimensional AMC complex, e.g., by choosing group generators in the support of each element, e.g., $a_j = 1 + x_j +$ (other monomials). Clearly, the second transformation changes the group presentation and the basis vectors associated with the lattice.

For example, with weight-two elements $a_i = 1 + x_i$, $1 \le i \le D$, we get a complex locally equivalent to D-dimensional QHP codes. Assuming the entire group can be generated this way [41],

$$G = \left\langle \{x_j\}_{j=1}^{D} \right\rangle,$$

we get a D-complex locally equivalent to D-dimensional toric codes. With a quantum CSS code associated with level-j subspace, for errors with irreducible weight smaller than the injectivity radius r_{inj}, this guarantees identical syndrome weights, that is, identical confinement profiles [22] up to r_{inj}. We also expect the code distance to grow as $d = \mathcal{O}(r_{\text{inj}}^{\alpha})$, with the exponent $\alpha = \min(j, D-j)$ expected for level-j D-dimensional toric codes, see Statement 4. Further, we can use a measuring circuit designed for a regular level-j D-dimensional toric code: its validity is guaranteed as a local property [42].

In practice, especially if we want to search for AMC chain complexes constructed from group algebra elements with weights higher than two and groups with two or more generators, it may be more efficient to go over small-weight polynomials and suitable periodicity vectors. For example, such a method was used in Ref. [30] to construct a number of weight-six locally planar GB (also known as BB) codes.

D. Matrix ranks for AMC construction

While the ranks of the matrices can be computed numerically in each particular case (e.g., with the help of Gauss elimination algorithm over the field F, or by analyzing the polynomial equations directly by constructing the corresponding Gröbner bases [43]), we have analytically computed the corresponding ranks in two cases.

First, consider a cyclic group of order ℓ, with the group algebra $F[C_\ell]$ isomorphic to the ring $F[x]/(x^\ell - 1)$ of modular polynomials. Here, the ranks of the boundary operators in the D-complex $\mathrm{AMC}(a_1, a_2, \ldots, a_D)$ constructed from single-variate polynomials $a_j \equiv a_j(x)$, $1 \le j \le D$, are expressed in terms of the *characteristic polynomial*,

$$h(x) = \gcd(a_1, a_2, \ldots, a_D, x^\ell - 1). \tag{32}$$

In Appendix A, we prove the following statement:

Statement 2. Consider a D-complex $\mathrm{AMC}(\{a_j\}_{j=1}^{D})$ over $F[C_\ell]$. The ranks of the boundary operators satisfy $\mathrm{rank}\, Q_j = \binom{D-1}{j-1}(\ell - \kappa)$, where $\kappa = \deg h(x)$ is the degree of the characteristic polynomial equation (32).

As an immediate consequence, the corresponding homology groups have orders $|H_j(\mathcal{Q})| = \binom{D}{j}\kappa$. Previously, the same or equivalent results were derived for

the special case of $D = 2$ AMC codes (quasi-cyclic GB codes), see Refs. [24,44]. Also note a similarity with the corresponding equations for D-dimensional QHP codes. The main difference with Eqs. (16) and (17) is the linear scaling with the group order ℓ, which is why the AMC construction gives much smaller codes.

Second is the case of a semisimple group algebra $F[G]$ where, according to Maschke's theorem, the group order $\ell = |G|$ is mutually prime with the field characteristic p, $\gcd(p, \ell) = 1$ (see, e.g., Corollary 2.2.5 in Ref. [45]). In this case, the result is very similar to that in Statement 2, except the value of κ is defined differently. For a technical definition of κ in terms of products of idempotent matrices, please see the proof given in Appendix B. In practice, κ can be defined, e.g., as the dimension of the classical F-linear code with the check matrix Q_D (all D square blocks stacked together in a single column block).

Statement 3. Consider a D-dimensional complex $\mathcal{Q} = \mathrm{AMC}(a_1, a_2, \ldots, a_D)$ over a semisimple abelian group algebra $F[G]$. The ranks of all boundary operators are proportional to that of Q_D, $\operatorname{rank} Q_j = \binom{D-1}{j-1} \operatorname{rank} Q_D$.

The same result can be also proven using a decomposition of the semisimple abelian group G into a product of semisimple cyclic groups, see the Appendix in Ref. [46].

E. Distance bounds

First, we construct lower (existence) bounds on homological distances in AMC complexes. They are based on the results for D-dimensional QHP codes [20,21,35], and the fact that the AMC construction includes QHP codes derived from abelian group-algebra codes as a special case. We prove in Appendix C:

Statement 4. Let G be a finite abelian group presented with the list of generators $\boldsymbol{x} = (x_1, x_2, \ldots, x_m)$, and $K \equiv G^{\times D}$ its D-fold tensor product with itself, with the corresponding list of generators $\{\boldsymbol{x}_1, \boldsymbol{x}_2, \ldots, \boldsymbol{x}_D\}$. Given a checkable [36] abelian group-algebra code in $F[G]$ of length n, dimension k, and distance d, with the orthogonal element $a \equiv a(\boldsymbol{x})$, consider the group algebra elements $a_i \equiv a(\boldsymbol{x}_i) \in F[K]$, $1 \le i \le D$, and the corresponding D-complex $\mathcal{Q} = \mathrm{AMC}(a_1, a_2, \ldots, a_D)$. Its jth subspace has dimension $n_j \equiv \dim(\mathcal{Q}_j) = \binom{D}{j} n^D$, while the corresponding homology and co-homology groups have the same dimension $k_j = \binom{D}{j} k^D$ and homological distances $d_j = d^j$ and $\tilde{d}_j = d^{D-j}$, respectively.

In the special case of a symmetric $D = 2j$ AMC code at level j, this gives the encoding rate $k_j/n_j = (k/n)^D$ and the distance $d^{D/2}$. Thus, a finite rate and a linear distance scaling in the original code family would give a finite rate and the distance scaling as a square root of the code length, similar to GB codes equivalent to QHP codes. While we are not aware of a proof that good linear abelian group-algebra codes exist (known results include good code families based on *non-abelian* dihedral groups D_{2m} [47], random quasi-abelian codes [48], and nonlinear cyclic codes [49] that attain the Gilbert-Varshamov bound), already the classical results on cyclic codes [50,51] are sufficient to show the existence of AMC codes with finite relative distances and power-law distance scaling, with the exponent arbitrarily close to $1/2$.

Second, we give an upper bound on the distance for any AMC code based on a cyclic group. The bound, formulated in terms of the characteristic polynomial equation (32) is a generalization of a similar result for GB codes [26].

Statement 5. Take a D-complex $\mathcal{Q} = \mathrm{AMC}(\{a_i\}_{i=1}^D)$ over $F[C_\ell]$ with characteristic polynomial $h(x)$. Let $d_h^\perp$ be the minimal distance of the F-linear cyclic code with the check polynomial $h(x)$. The homological distances satisfy the inequality $d_j(\mathcal{Q}) \le d_D(\mathcal{Q}) = d_h^\perp$, $1 \le j < D$.

When boundary operators from a level-j homology group are used to construct a CSS code, this gives a uniform upper bound on the code distances, $d \le d_h^\perp$. We also get a bound on the single-shot distance [14] $d_{\mathrm{SS}} \le d_h^\perp$, a parameter which may be relevant when the code is operated in a fault-tolerant setting.

Notice, however, that the single-shot distance d_{SS} is only relevant if data and syndrome decoding are done separately, and that only if we are using unmodified matrices from the chain complex, e.g., $M_X = Q_{j-1}$ and $M_Z = Q_{j+2}^T$, with $H_X = Q_j$ and $H_Z = Q_{j+1}^T$. In practice, the single-shot distance may be increased by adding homologically nontrivial chains (co-chains) as additional rows of M_X (M_Z). The downside is that these vectors may have higher weights, potentially increasing the complexity of the syndrome decoding step.

Another parameter relevant in a fault-tolerant setting is the *syndrome distance* d_{S}, the minimum weight of a nonzero syndrome vector. An obvious upper bound is the minimum column weight in the check matrix. A boundary operator Q_j in an AMC D-complex $\mathcal{Q}$ has j or $D+1-j$ nonzero blocks in each block column or row, respectively. If we use group algebra elements of the same weight ω, this gives uniform column weights $j\omega$ and row weights $(D+1-j)\omega$. For a code $\mathrm{CSS}(Q_j, Q_{j+1}^T)$ in the space $\mathcal{Q}_j$ of such a D-complex, this gives a simple upper bound on the syndrome distance,

$$d_{\mathrm{S}} \le \min(j, D-j)\omega. \tag{33}$$

We also get uniform weights of the stabilizer generators defined by the rows of $H_X = Q_j$ and $H_Z = Q_{j+1}^T$,

$$w_X = (D+1-j)\omega, \quad w_Z = (j+1)\omega. \tag{34}$$

In particular, with $D = 4$ and $j = 2$, this gives an upper bound for the syndrome distance $d_S \leq 2\omega$ and stabilizer generators of a uniform weight $w_X = w_Z = 3\omega$.

IV. NUMERICAL RESULTS

A. Family of four-dimensional rotated toric codes

We now focus on the family of quasicyclic CSS codes $\mathrm{AMC}_2(a_1, a_2, a_3, a_4)$ constructed from distinct weight-2 group algebra elements $a_i \in F[C_\ell]$, $1 \leq i \leq 4$. As explained in the previous section, such codes are locally equivalent to 4-dimensional toric codes with qubits on faces (second homology group). While the topology of the code is the same as for the regular 4D toric codes, the lattice periodicity vectors $\mathbf{\Delta}_i$ need no longer be parallel to the Cartesian axes. Thus, we may refer to these codes as *rotated 4D toric codes*.

Specifically, we constructed such codes for $7 \leq \ell \leq 30$ and corresponding block lengths $n = 6\ell$ (four distinct weight-2 polynomials cannot be found for $\ell < 7$). Generating polynomials and parameters of smallest codes for each minimum distance d are listed in Table I. All constructed codes have the same dimension $k = 6$ and the same characteristic polynomial $h(x) = 1 + x$. For comparison, in Table I, we also list parameters of two conventional 4D toric codes, which require larger block lengths to achieve the same distances.

In addition to code parameters and the defining polynomials, Table I shows the confinement profiles [22] of the constructed codes, computed using the dist_m4ri program [52]. The confinement profile $w_S(x)$ is defined as the minimum syndrome weight for an error e with irreducible weight $x = 1, 2, \ldots$. Here, the irreducible weight $x = w(e)$ is the minimum weight of an error equivalent to e. For any nonzero $x < d$, the confinement profile is bounded from below by the syndrome distance, $w_S(x) \geq d_S$, while $w_S(0) = w_S(d) = 0$, where d is the code distance.

As discussed in Sec. III C, AMC codes constructed from polynomials of weight two are locally equivalent to higher-dimensional toric codes. They have identical confinement profiles, up to the injectivity radius. In particular, for a $4D$ toric code with qubits on the plaquettes, codewords are two-dimensional membranes; creation of a (partial) membrane of radius r and area $\mathcal{O}(r^2)$ requires perimeter (syndrome weight) linear in r, which implies a square root scaling for the confinement profile, $w_S = \mathcal{O}(w^{1/2})$, for error weights $w \leq w_{\max} = \mathcal{O}(L^2)$. For such a code with block size $n = 6L^4$, the code distance is $d = L^2$, while the energy barrier (maximum of the confinement profile) scales as $\mathcal{O}(L) = \mathcal{O}(n^{1/4})$.

For a large $4D$ toric code, the first five terms in the confinement profile $w_S(x)$ are $4, 6, 6, 8, 8$. Only the first couple of terms of the confinement profiles of the larger AMC codes in Table I match this sequence, consistent with the fact that injectivity radii for these codes are small. For example, for the code with $\ell = 30$, if we follow the prescription in Sec. III C and define the generators $x_1 = x^2$, $x_2 = x^5$, $x_3 = x^8$, and $x_4 = x^9$, we get a periodicity vector of length $2r_{\mathrm{inj}} = 6^{1/2} < 3$, as follows from the relation

$$x_1^2 x_2 x_4^{-1} \equiv (x^2)^2 x^5 x^{-9} = 1,$$

between thus defined generators. Nevertheless, the confinement profiles for the codes in Table I are higher than, e.g., for $3 + 3$ GB codes with syndrome distance $d_S = 3$ previously studied in Ref. [25], where the confinement profiles necessarily start with $3, 4, 3$, increasing only for irreducible error weights $x \leq 2$.

B. Circuit design

Stabilizer generator matrices of these codes, $H_X = R_2$ and $H_Z = R_3^T$ are shown in Eqs. (27) and (28), where the blocks A, B, C, and D should be replaced with the

TABLE I. Smallest $D = 4$ AMC_2 qubit codes (rotated 4D toric codes) with increasing distances d, constructed from cyclic groups C_ℓ with $\ell \leq 30$ (above the line) and two conventional 4D toric codes (below the line). Confinement profile [22] ("confin") column lists the minimum syndrome weights for irreducible errors of weights from 1 to 5, except for codes with $\ell = 7$ and $\ell = 2^4$, where the biggest irreducible errors have weights 4 and 3, respectively.

ℓ	n	k	d	d_S	a_1	a_2	a_3	a_4	confin
7	42	6	4	4	$1+x$	$1+x^2$	$1+x^3$	$1+x^4$	4, 4, 4, 6
10	60	6	5	4	$1+x$	$1+x^2$	$1+x^3$	$1+x^4$	4, 6, 6, 6, 4
11	66	6	6	4	$1+x$	$1+x^2$	$1+x^3$	$1+x^4$	4, 6, 6, 6, 4
14	84	6	7	4	$1+x$	$1+x^2$	$1+x^5$	$1+x^6$	4, 6, 6, 6, 4
16	96	6	8	4	$1+x$	$1+x^3$	$1+x^5$	$1+x^7$	4, 6, 8, 8, 4
18	108	6	9	4	$1+x$	$1+x^3$	$1+x^5$	$1+x^7$	4, 6, 8, 8, 4
25	150	6	10	4	$1+x$	$1+x^4$	$1+x^6$	$1+x^9$	4, 6, 8, 8, 4
28	168	6	11	4	$1+x$	$1+x^3$	$1+x^7$	$1+x^{12}$	4, 6, 8, 8, 4
30	180	6	12	4	$1+x^2$	$1+x^5$	$1+x^8$	$1+x^9$	4, 6, 8, 8, 4
2^4	96	6	4	4	$1+x_1$	$1+x_2$	$1+x_3$	$1+x_4$	4, 4, 4
3^4	486	6	9	4	$1+x_1$	$1+x_2$	$1+x_3$	$1+x_4$	4, 6, 6, 8, 4

corresponding circulant matrices. With weight-two polynomials, $\omega = 2$, this gives stabilizer generators of uniform weight $w_X = w_Z = 6$. Each data qubit (associated with a plaquette on a hypercubic lattice) is neighboring with four X checks (edges) and four Z checks (cubes), total of 8 checks.

We have set out to design quantum codes with increased redundancy of low-weight stabilizer generators. Evidently, constructed matrices have *too much redundancy* to measure all checks in a circuit of optimal duration. For this reason, in each round of measurement, we chose to address only the stabilizer generators corresponding to three chosen row blocks, labeling the corresponding circuits by the index of the dropped row block.

As an example, after removing the first and the last row blocks, respectively, from the CSS matrices $H_X = R_2$ and $H_Z = R_3^T$ in Eqs. (27) and (28), we get in the case of a binary field,

$$H_X^{(1)} = \left[\begin{array}{ccc|ccc} D_1 & & & B_4 & A_5 & \\ & D_2 & & C_4 & & A_6 \\ & & D_3 & & C_5 & B_6 \end{array}\right], \tag{35}$$

$$H_Z^{(1)} = \left[\begin{array}{ccc|ccc} \widehat{B}_1 & \widehat{C}_2 & & \widehat{D}_4 & & \\ \widehat{A}_1 & & \widehat{C}_3 & & \widehat{D}_5 & \\ & \widehat{A}_2 & \widehat{B}_3 & & & \widehat{D}_6 \end{array}\right], \tag{36}$$

where the subscripts next to block names label the columns and the circumflex "hat" accent indicates transposed blocks. Focusing on bigger 3×3 blocks, we have a two-block structure similar to that in lifted-product or GB/2BGA codes, with two and four ("$2 + 4$") nonzero entries in each subrow. The circuits designed [25] for $2 + 4$ 2BGA/GB codes, a generalization of the N-Z addressing scheme [53] for rotated surface codes, also work in the present case. A valid time-optimal circuit is obtained if we address the qubits corresponding to the two terms in the D blocks at steps 1 and 6 (first and last), with the opposite order for H_X and H_Z, while addressing the qubits from the remaining blocks in the intervening time steps. Specifically, we used the following addressing scheme:

H_X	D_{10}	B_{40}	B_{41}	A_{50}	A_{51}	D_{11}
	D_{20}	A_{60}	A_{61}	C_{40}	C_{41}	D_{21}
	D_{30}	C_{50}	C_{51}	B_{60}	B_{61}	D_{31}
H_Z	$\widehat{D}_{41}$	$\widehat{B}_{10}$	$\widehat{B}_{11}$	$\widehat{C}_{20}$	$\widehat{C}_{21}$	$\widehat{D}_{40}$
	$\widehat{D}_{51}$	$\widehat{C}_{30}$	$\widehat{C}_{31}$	$\widehat{A}_{10}$	$\widehat{A}_{11}$	$\widehat{D}_{50}$
	$\widehat{D}_{61}$	$\widehat{A}_{20}$	$\widehat{A}_{21}$	$\widehat{B}_{30}$	$\widehat{B}_{31}$	$\widehat{D}_{60}$

Here, each column corresponds to a circuit time step, and each row to a block row of the matrices Eqs. (35) and (36), with secondary subscripts labeling the location corresponding to a free term ("0") and the other monomial ("1"). For example, the first row indicates that for measuring stabilizer generators defined by the first row block of Eq. (35), one should first address the qubit corresponding to the free term (second subscript 0) of the polynomial defining the D_1 block, then the free term (second subscript 0) of the B_4 block, then the other monomial (second subscript 1) of the same block, etc. Circuits corresponding to the original matrices with second, third, or fourth row removed were constructed identically, with the help of column permutations rendering the matrices in the form of Eqs. (35) and (36), up to block labels.

Based on this addressing scheme for a single measurement round, we designed three types of four-round syndrome measurement circuits, 1111, 1212, and 1234 [54]. Here, a digit stands for the row omitted in each particular round of measurement, and we constructed detector events matching pairs of closest available measurement outcomes, either from neighboring or next-nearest-neighboring rounds. Overall, all our circuits have fixed duration of $T_{\max} = 9$ measurement rounds, including two four-round cycles and a final measurement of all data qubits in Z or X basis, depending on the initial state of the data qubits, $|0\rangle^{\otimes n}$ or $|+\rangle^{\otimes n}$. The results of the final measurement are combined to construct the final set of detector events (thus computed syndrome bits are exact), and also the logical observables which are used to verify whether the decoding was successful.

C. Circuit simulation results

Thus, designed measurement protocols have been implemented as Stim circuits [55], using CX and XCX gates, with a standard circuit error model. We included probability-p single-qubit depolarizing noise on the data qubits at the start of each round, two-qubit depolarizing noise with probability p after every two-qubit gate, and also bit-flip (phase-flip) Pauli error channel with the same probability p before and after each Z-basis (X-basis) measure-reset (MR) gate. There are no single-qubit gates in our circuits, and we chose to omit errors for idling intervals due to the fact that in most platforms single-qubit Clifford gates and idle intervals have error rates small compared to those of two-qubit entangling gates or single-qubit MR operations.

For accurate decoding, one needs to know probabilities of individual faults in the circuit and their effects on the detectors and the logical observables. This information for a given circuit is computed automatically by Stim, which also aggregates the faults producing the identical effect, and can be exported as a detector error model (DEM) file [55]. Information about aggregated faults in a DEM file can be regarded as columns of stabilizer-generator H_X and logical L_X matrices (with known aggregated fault probability for each column) for an asymmetric quantum CSS code. In particular, the distance d_Z of this code is identified as the

circuit distance. We used vecdec program [56] to export the matrices from the DEM files associated with individual circuits, and dist_m4ri program to compute the corresponding distances (with the distances $d \leq 6$ computed exactly with a greedy enumeration algorithm, and upper bounds for larger distances using a random information set algorithm [57], exact with a high probability).

Circuit simulations have been done with Pauli-frame circuit simulator Stim [55] written by Craig Gidney, and the decoding using vecdec program [56]. Specifically, before attempting belief-propagation (BP) decoding, the program tries to match the syndrome data against a precomputed list of small-weight error clusters; such a simple pre-decoder gives a substantial acceleration, especially at smaller error probabilities. If pre-decoding fails, the corresponding clusters are discarded, and a BP decoder with serial schedule, using both average and instantaneous logarithmic likelihood ratios (whichever converges first) is engaged, with up to 50 steps. Finally, if that fails, the logarithmic likelihood ratios (LLRs) are transmitted to the OSD-1 decoder. A sample of circuit simulation data for codes $[[42, 6, 4]]$, $[[66, 6, 6]]$, and $[[96, 6, 8]]$ (see Table I), with the standard error model described earlier and the "1212" syndrome-addressing cycle, is shown on a threshold-style plot in Fig. 1. To speed up the decoding, we simplified the DEM by dropping all "minority" detector events, which somewhat increases logical error rates [58]. Nevertheless, asymptotic slopes at small p consistent with $d/2$ (where d is the code distance) are in agreement with the circuit distances computed independently. The (pseudo)threshold position (crossing point) is at $p_c \approx 1.1\%$, in approximate agreement with the circuit

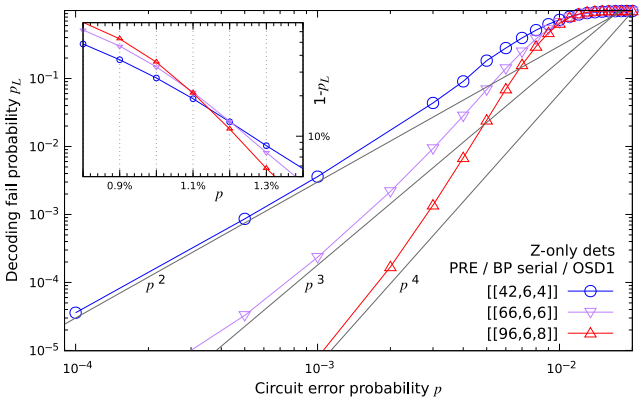


FIG. 1. Logical error rate as a function of the circuit noise parameter p, using the syndrome-addressing scheme "1212" and Z-basis final measurements. For faster simulations, only Z-measurement detector events have been included. Results for short even-distance codes $[[42, 6, 4]]$, $[[66, 6, 6]]$, and $[[96, 6, 8]]$ (see Table I) are shown. Inset shows the success probability $1 - p_L$ as a function of p in the vicinity of the crossing point(s) at $p \approx 1.1\%$.

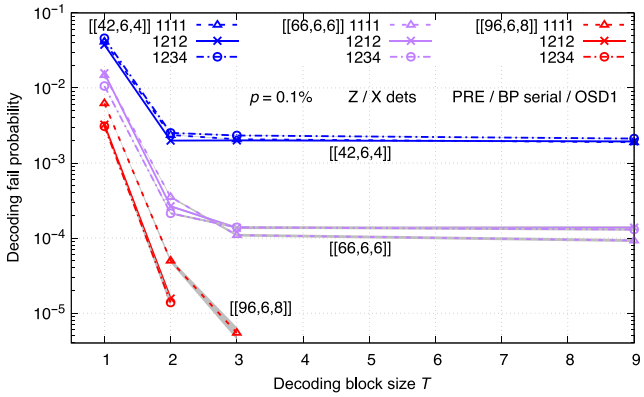


FIG. 2. Logical error rates computed with full detector error models (both X and Z detector events) for the same codes as in Fig. 1, plotted as a function of the decoding window size T. Shading indicates the statistical error at one standard deviation. Here, $T = T_{\max} = 9$, the total number of measurement rounds in our circuits, corresponds to (most accurate) full-block decoding, while $T < T_{\max}$ are the number of rounds used in sliding-window decoding protocols. The data labeled as "1111", "1212", and "1234" correspond to different syndrome measurement cycles as explained in the text. At larger T, syndrome measurement errors are less important, and the "1111" cycle gives lower error rates due to shorter measurement cycle. In contrast, with single- ($T = 1$) and two-shot ($T = 2$) decoding, the error rates are lower with the other two cycles which better utilize the syndrome redundancy. In comparison, in the "1111" measurement cycle, most of the redundant checks are discarded. The difference is substantial for the code $[[96, 6, 8]]$ with a larger minimal distance $d = 8$, see a discussion in Sec. IV D.

simulation results for similar codes in Ref. [34]. We note that our value is (marginally) higher than the values for toric and surface codes under the same error models.

In addition, to illustrate the "single-shot" properties of the constructed codes, we have tried sequential one-step SW decoding [18,23,59], with windows of different sizes. Details of our implementation are given in Ref. [25]. Some simulation results for the same three codes as in Fig. 1 are shown in Fig. 2, where the logical error rates p_L are plotted as a function of the decoding window size T at a fixed circuit error rate, $p = 10^{-3}$. Up to 5×10^6 samples have been generated for each point, resulting in very small statistical errors.

For the data in Fig. 2, we used full DEMs for decoding, including the detector events associated with both X- and Z-measurements, which resulted in somewhat lower p_L at full-block decoding ($T = 9$) than those in Fig. 1 at the same p. For each code, we tried all three syndrome measurement cycles. Simplest is the "1111" cycle, where the same three row blocks are measured in each round. While discarding most of the redundant generators, this cycle is the most accurate with full-block decoding. In comparison, the "1234" cycle which addresses most uniformly all low-weight stabilizer generators, gives the lowest fail rates with

single-shot ($T = 1$) and two-shot ($T = 2$) decoding protocols. Note that only during the rounds labeled with "1" a full-rank set of stabilizer generators is measured.

D. Discussion of the simulation results

First, we note that LDPC codes, quantum or classical, have Tanner graphs of bounded degree. Consequently, a high-weight stochastic error—even one exceeding the code distance—can be decomposed into a collection of smaller, localized clusters. These clusters can then be decoded independently [60,61]. Fault-tolerant circuit detector error models (DEMs) for LDPC codes inherit this same property of locality.

For such a code or circuit with distance d and a sufficiently small error probability p, the logical error probability under minimum-weight decoding scales as

$$P_{\text{fail}} = AN \binom{d}{t+1} p^{t+1}.$$

Here, A is an order-one prefactor, $t \equiv \lfloor (d-1)/2 \rfloor$ is the number of corrected errors, and the binomial factor represents the number of failing configurations within a codeword. N denotes the number of irreducible codewords, where a fault of $t+1$ errors can cause a decoding failure. Specifically: when $d = 2t+2$ (even), N is the number of minimum-weight codewords; when $d = 2t+1$ (odd), N can be estimated as the number of codewords with weights d and $d+1$. For precise definitions of these terms, see Ref. [61].

A sliding window decoder is inherently suboptimal compared to a full-circuit decoder, and its decoding accuracy worsens with the decreasing window size T. Depending on the code at hand, such a decoder may fail for certain errors of weight $t' + 1 < t + 1$, leading to an asymptotically higher logical error rate $P_{\text{fail}} = \mathcal{O}(p^{t'+1})$. Alternatively, it may fail only on additional error configurations of the same weight $t+1$; this results in a similar scaling at small p but with an increased prefactor $N' > N$. For surface codes, a window size of $T \geq d$ is sufficient to achieve optimal decoding accuracy [62,63].

One mechanism that can cause a dramatic increase in the prefactor N (at fixed t) for small window sizes is the LDPC-breakdown transition [25]. Consider an error e with irreducible weight $w \equiv \text{wgt}(e)$ and syndrome weight w_s (the number of detectors flipped in a single measurement round). A one-step sliding window (SW) decoder with window size T, using minimum-weight decoding, will misinterpret the entire error e as a sequence of measurement errors if

$$w_s T < w. \tag{37}$$

Such an error is perpetuated until the final round of measurement where it is corrected. While this effect alone does not reduce the circuit distance, it creates a vulnerability. In codes with a flat energy profile, LDPC breakdown allows a chain of additional, infrequent weight-one errors to eventually trigger a decoding failure. This increase in the number of failing error configurations is entirely entropic. In contrast, with larger T, a decoding failure typically requires a weight-$(t+1)$ error to be localized within a single measurement cycle. Notably, a high energy barrier or a high confinement profile suppresses this process, as additional data errors that increase w may eventually violate condition (37), allowing the decoder to correctly identify and resolve the error.

SW decoding with a smaller T can also be viewed as a variant of local decoding. The most well-understood analogue is finite-temperature self-correction in a Hamiltonian model corresponding to a code, which is quantified by the code's energy profile and energy barrier [64]. For a surface code the energy profile is flat, $w_s(x) = 1$. Consequently, once a weight-one error is created, additional errors can be added without penalty, effectively diffusing the endpoint of a string-like fault through the system and rendering such codes unstable at finite temperatures. In contrast, 4D toric codes exhibit self-correction. Their energy profile is lower-bounded by a confinement profile scaling as $w_S(x) = \mathcal{O}(x^{1/2})$, with an energy barrier scaling as $\mathcal{O}(L) = \mathcal{O}(n^{1/4})$. As a result, local decoders are efficient for such codes [65]. For 4D AMC codes—such as those constructed from weight-2 polynomials—we expect properties similar to 4D toric codes (up to the injectivity radius) when all minimum-weight stabilizer generators are measured. Furthermore, single-shot decoding and the associated sustained thresholds can be analyzed using the techniques proposed in Ref. [22].

In practice, we do not have a time-optimal scheme to measure the entire set of 4ℓ minimum-weight stabilizer generators at once. Instead, each measurement round only accesses generators in three row blocks of CSS matrices. When we address the same three row blocks in every measurement round (the data labeled "1111" in Fig. 2), we get a code with CSS matrices (35) and (36), with the same energy profile as for the toric code, $w_S(x) = 2$, due to the overall parity in the D blocks. Conversely, for the "1212" and "1234" circuits, some of the measurements are only verified after skipping a cycle. For these circuits, we expect the confinement profiles in Table I to become fully relevant only for SW decoding with $T \geq 2$.

How do we interpret the results in Fig. 2? For the circuits used, we have verified that our SW decoder with $T \geq 2$ preserves the code distance, i.e., it corrects any $t = 1$, 2, and 3 circuit errors for the three codes with distances $d = 4$, 6, and 8, respectively. Evidently, for all $d = 4$ circuits, SW decoding with $T = 2$ is sufficient to reach nearly the same accuracy as for $T = 9$ full-block decoding. For the $d = 6$ circuits, $T = 3$ gives results nearly identical to $T = 9$, with slightly lower logical error rates observed

for the shorter measurement cycle labeled "1111". The decoding failure probability increases as window size is decreased to $T = 2$, and here it is highest for the "1111" cycle—a result consistent with the expectation that the other two cycles offer better stability against measurement errors. For the $d = 8$ circuits, we see an even more pronounced increase of the logical error rates for $T = 2$ compared to $T = 3$ SW decoding (under the "1111" cycle), as well as compared to the $T = 2$ data for the other two cycles.

We notice that for the "1111" circuit, characterized by a flat effective confinement profile $w_S(x) = 2$, for a window size $T = 2$, Eq. (37) predicts a potential LDPC-breakdown transition only for errors of weight $w > 4$. A tie occurs at $w = 4$, which may be broken by our decoder if those specific syndrome errors are statistically more likely. It is apparent from Fig. 2 that this effect is sufficient to increase the prefactor N by a factor of two or three.

Clearly, while one- or two-shot decoding may function for the codes examined, it may not yield optimal error rates as the code distance increases. Larger decoding window sizes $T(x)$ may be necessary to ensure that the LDPC-breakdown transition does not occur for errors of weight x. For a power-law confinement profile $w_S(x) = \mathcal{O}(x^\alpha)$, Eq. (37) indicates that $T(x) = \mathcal{O}(x^{1-\alpha})$ is sufficient to prevent the breakdown transition. For larger 4D toric codes and locally equivalent AMC codes with the confinement exponent $\alpha = 1/2$, choosing $T = \mathcal{O}(d^{1/2})$ should be sufficient to fully suppress LDPC breakdown.

This argument also implies that linear confinement, $\alpha = 1$, would be sufficient to ensure that large codes within a family achieve their design error rates with a constant window size, $T = \mathcal{O}(1)$. This result aligns with the claim that linear confinement guarantees single-shot fault-tolerant decoding in the presence of stochastic errors [22].

V. CONCLUSION

In conclusion, we constructed a family of quantum error-correcting codes whose main advantage is a highly redundant set of minimum-weight stabilizer generators, with relatively short block lengths. Just like the higher-dimensional QHP codes which our codes generalize, the construction defines a sequence of chain complexes of varying lengths. The constructed D-dimensional codes are highly symmetric and they are characterized by confinement profiles and single-shot properties similar to those of the D-dimensional QHP codes.

It is instructive to compare the parameters of D-dimensional AMC codes over $F[C_\ell]$ with a characteristic polynomial $h(x)$, and D-dimensional QHP codes constructed from a linear cyclic code with parameters $[\ell, \kappa, \delta]$ and the same check polynomial $h(x)$. At level j, the QHP code has block length $N = \binom{D}{j}\ell^D$, dimension $K = \binom{D}{j}\kappa^D$, and minimal distance $\min(\delta^j, \delta^{D-j})$, i.e., its rate scales as a power of that of the original code, $R = (\kappa/\ell)^D$. In comparison, the block lengths and the dimensions of AMC codes scale linearly with ℓ, $n = \binom{D}{j}\ell$ and $k = \binom{D}{j}\kappa$, so that the rate does not change, which is also a feature of GB codes.

While there is no explicit expression for the distance, we can use the codes in Table I to compare the actual distances with the corresponding upper bounds from Statement 5, which for these codes are given by the block size, ℓ. For $d \le 9$, we have a reasonably good linear scaling, $d \ge \ell/2$, while for the remaining three codes, $d > \ell/3$. (Unfortunately, we do not expect the distances to remain as high for larger codes.)

The most important property of the proposed construction is the high redundancy of its minimum-weight stabilizer generators. For a quasi-abelian two-block code of dimension $k = 2\kappa$, there are exactly κ minimum-weight redundant generators of each type (X and Z). In contrast, the stabilizer generator matrices of a symmetric AMC code with even $D = 2j$ have ranks $\binom{2j-1}{j-1}(\ell - \kappa)$ and possess $\binom{2j}{j-1}\ell$ rows. This provides a redundancy of over 25% for $D = 4$ and over 33% for $D = 6$. Such redundancy can be leveraged to accelerate decoding and improve accuracy under realistic circuit noise. This is illustrated by our simulations of relatively short AMC codes, which demonstrate two-shot decoding comparable in accuracy to full-block decoding. We also find a pseudothreshold above 1%—exceeding those of surface codes (with weight-4 generators) and GB codes with weight-6 generators. Further studies are required to establish the long-term performance of the constructed codes; in particular, how sustained error rates depend on the decoding window size T.

ACKNOWLEDGMENTS

This work was supported in part by the APS M. Hildred Blewett Fellowship (HKL), and the NSF Awards No. 2112848 (L.P.P.) and No. OIA-2044049 (A.A.K.).

DATA AVAILABILITY

The data that support the findings of this article are not publicly available because of legal restrictions preventing unrestricted public distribution. The data are available from the authors upon reasonable request.

APPENDIX A: PROOF OF STATEMENT 2

The calculation is based on the fact that the group algebra $F[C_\ell]$, isomorphic to the ring $R \equiv F[x]/(x^\ell - 1)$ of modular polynomials, is a gcd domain. That is, for any two polynomials $a(x), c(x) \in F[x]/(x^\ell - 1)$, there exists a polynomial $h_{ac}(x) \equiv \gcd(a, c) \in R$, the greatest common divisor of the two original polynomials. Moreover, there also exist Bézout coefficients $u(x), v(x) \in F[x]/(x^\ell - 1)$

such that

$$u(x)a(x) + v(x)c(x) = h_{ac}(x) \equiv \gcd(a, c). \tag{A1}$$

Equivalently, if we introduce the rescaled polynomials $a'(x) = a(x)/h_{ac}(x)$, $c'(x) = c(x)/h_{ac}(x)$, this gives $u(x)a'(x) + v(x)c'(x) = 1$. Rescaled polynomials and the Bézout coefficients can be used to construct unimodular (and thus invertible) matrices,

$$M_{\pm}(x) = \begin{pmatrix} a'(x) & \pm c'(x) \\ \mp v(x) & u(x) \end{pmatrix}, \quad \det M_{\pm} = 1.$$

The corresponding two-block matrices are also invertible,

$$\hat{W}_{\pm} = \begin{pmatrix} A' & \pm C' \\ \mp V & U \end{pmatrix}, \quad \hat{W}_{\pm}^{-1} = \begin{pmatrix} U & \mp C' \\ \pm V & A' \end{pmatrix},$$

where $A' = \mathrm{M}(a')$, $C' = \mathrm{M}(c')$, etc. are $\ell \times \ell$ circulant matrices constructed from the corresponding polynomials; we have $AC' - CA' = 0$ and $UA + VC = H_{ac} \equiv \mathrm{M}(h_{ac})$.

Our approach is to construct a sequence of row and column transformations diagonalizing the boundary operator matrices in an AMC complex. First, demonstrate the steps on the first two matrices in the 3-complex $\mathcal{R} = \mathrm{AMC}(a, b, c)$, see Eqs. (20) and (21). Here, we want to eliminate matrices $C = \mathrm{M}(c)$, while replacing all matrices A with $H_{ac} = \mathrm{M}(h_{ac})$. To this end, denote $W^{\pm}_{i,j}$ the unimodular block-diagonal matrices constructed from an identity matrix by replacing blocks in positions $\{(i,i),(i,j),(j,i),(j,j)\}$ with the blocks of the corresponding matrices $\hat{W}_{\pm}$ (row-first order), $\overline{W}^{\pm}_{i,j}$ the corresponding inverse matrices, and $\underline{W}^{\pm}_{i,j}$, $\overline{\underline{W}}^{\pm}_{i,j}$ the same matrices with additional sign-flip. Explicitly,

$$Q'_1 = Q_1 \overline{W}^{+}_{31} = [C, B, A] \begin{bmatrix} A' & & V \\ & I & \\ -C' & & U \end{bmatrix} = [0, B, H_{ac}],$$

$$Q'_2 = W^{+}_{3,1} Q_2 \overline{W}^{-}_{3,1}$$
$$= \begin{bmatrix} +U & & -V \\ & I & \\ +C' & & +A' \end{bmatrix} \begin{bmatrix} B & A & 0 \\ -C & 0 & A \\ 0 & -C & -B \end{bmatrix} \overline{W}^{-}_{3,1}$$
$$= \left[\begin{array}{ccc} UB & H_{ac} & VB \\ -C & 0 & A \\ C'B & 0 & -A'B \end{array}\right] \begin{bmatrix} A' & & -V \\ & I & \\ C' & & U \end{bmatrix}$$
$$= \left[\begin{array}{ccc} B & H_{ac} & 0 \\ 0 & 0 & H_{ac} \\ 0 & 0 & -B \end{array}\right].$$

The matrices are now reduced to a block-diagonal form, with the blocks being the matrices from the 2-dimensional complex $\mathrm{AMC}(h_{ac}, b)$, which, with the help of the identity

$$\gcd(h_{ac}, b, x^{\ell} - 1) = \gcd(a, b, c, x^{\ell} - 1) \equiv h(x),$$

immediately gives

$$\operatorname{rank} Q_1 = \operatorname{rank} Q'_1 = \ell - \deg h = \ell - \kappa,$$
$$\operatorname{rank} Q_2 = \operatorname{rank} Q'_2 = 2(\ell - \deg h) = 2(\ell - \kappa).$$

The elimination process goes the same way for larger-D complexes. Due to symmetry, whenever a pair of matrices, say, A and B, are located in positions (x_1, y_1), (x_1, y_2) (same column) and in (x_2, y_3), (x_3, y_3) (same row), the corresponding 3×3 block (rows $\{y_1, y_2, y_3\}$, columns $\{x_1, x_2, x_3\}$) will necessarily have the form of Q_2 in Eq. (21), with only one additional block (e.g., C), up to some signs and the block labels.

We illustrate the elimination process on the example of the first two matrices from the 4-complex $\mathrm{AMC}(a, b, c, d)$ in Eqs. (26) and (27). Here, $ua + vd = h_{ad} \equiv \gcd(a, d, x^{\ell} - 1)$, $a' = a/h_{ad}$, $d' = d/h_{ad}$, and capital letters correspond to block matrices, $A' = \mathrm{M}(a')$, $U = \mathrm{M}(u)$, etc.

$$R'_1 = R_1 \overline{W}^{+}_{4,1} = [D, C, B, A] \begin{bmatrix} A' & & & V \\ & I & & \\ & & I & \\ -D' & & & U \end{bmatrix} = [0, C, B, H_1], \text{ and}$$

$$R'_2 = W^{-}_{4,1} R_2 \overline{W}^{-}_{5,1} \overline{W}^{-}_{6,2}$$
$$= \begin{bmatrix} U & & & -V \\ & I & & \\ & & I & \\ D' & & & A' \end{bmatrix} \left[\begin{array}{cccc} C & B & A & \\ -D & & & \\ & -D & & \\ & & -D & \end{array}\right.$$
$$\left.\begin{array}{ccc} & & \\ B & A & 0 \\ -C & 0 & A \\ 0 & -C & -B \end{array}\right] \overline{W}^{-}_{5,1} \overline{W}^{-}_{6,2}$$

$$= \left[\begin{array}{ccc|ccc} UC & UB & H_1 & 0 & VC & VB \\ -D & & & B & A & 0 \\ & -D & & -C & 0 & A \\ D'C & D'B & 0 & 0 & -A'C & -A'B \end{array}\right] \left[\begin{array}{cccc} A' & & & -V \\ & I & & \\ & & I & \\ & & & I \\ D' & & & U \\ & & & & I \end{array}\right] \overline{W_{6,2}}$$

$$= \left[\begin{array}{ccc|ccc} C & UB & H_1 & 0 & 0 & VB \\ 0 & & & B & H_1 & 0 \\ & -D & & -C & 0 & A \\ & D'B & 0 & 0 & -C & -A'B \end{array}\right] \left[\begin{array}{cccc} I & & & \\ & -V & & A' \\ & & I & \\ & & & I \\ & U & & D' \end{array}\right] = \left[\begin{array}{ccc|ccc} C & B & H_1 & & & \\ 0 & & & B & H_1 & 0 \\ & 0 & & -C & 0 & H_1 \\ & & 0 & 0 & -C & -B \end{array}\right].$$

The proof can be now completed recursively. Indeed, the rank expression in Statement 2 is valid for $D = 2$ which corresponds to a GB code based on a cyclic group. Assuming it is valid for some $D \geq 2$, take a circulant matrix $N = \mathrm{M}(n(x))$ and use Eqs. (23)–(25) to construct the boundary operators for the dimension $D+1$. Now, use the reduction protocol described to eliminate matrices N and replace $A \to \mathrm{M}(h_{a,n})$, where $h_{a,n} = \gcd(a, n, x^\ell - 1)$. By assumption, the ranks at level j are $\operatorname{rank} Q_j = \binom{D-1}{j-1}(\ell - \kappa)$, where $\kappa = \deg h(x)$, and the expression for the characteristic polynomial now includes all $D+1$ polynomials including $n(x)$. This gives

$$\begin{aligned} \operatorname{rank} R_j^{D+1} &= \binom{D-1}{j-2}(\ell-\kappa) + \binom{D-1}{j-1}(\ell-\kappa) \\ &= \binom{D}{j-1}(\ell-\kappa), \end{aligned}$$

in agreement with the assumption. This completes the induction.

APPENDIX B: PROOF OF STATEMENT 3

The proof is based on the following:

Lemma B1. For a D-complex $\mathcal{Q} = \mathrm{MBC}(A, B, \ldots)$, suppose one of the matrices, e.g., matrix A, which does not limit generality, can be factored out from the other matrices, that is, $B = B'A = AB'$, $C = C'A = AC'$, etc., then $\operatorname{rank} Q_j^{(D)} = \binom{D-1}{j-1} \operatorname{rank} A$.

Proof. Permute the terms in the product so that A enters last, and use Eqs. (23)–(25). The block $N = A$ enters Q_j only along the diagonal of the square block of block-dimension $\binom{D-1}{j-1}$; the remaining matrices are above and to the right. Using the assumed factorization, $B = B'A$, etc., row and column transformation can be used to diagonalize the matrix Q_j, leaving only the square block with A along the diagonal. This gives $\operatorname{rank} Q_j = \binom{D-1}{j-1} \operatorname{rank} A$. ■

Proof of Statement 3. By assumption, the group algebra $F[G]$ is semisimple; every ideal in such a group algebra is generated by an idempotent element. That is, for any $a \in F[G]$, there is an idempotent element $e_a \in F[G]$ (necessarily $e_a = e_a^2$) such that $e_a a = a$ and, necessarily, $(1 - e_a)a = 0$. Then, given $\{a, b, c, \ldots\} \subset F[G]$, construct the corresponding matrices $A = \mathrm{M}(a)$, $B = \mathrm{M}(b)$, etc, as well as the idempotent matrices $E_a = \mathrm{M}(e_a)$, $E_b = \mathrm{M}(e_b)$, etc; all of these matrices commute and satisfy, e.g., $E_A A = A E_A = A$, $(I - E_A)A = 0$. For a D-complex $\mathrm{AMC}(a, b, c, \ldots)$, there are D group algebra elements and D corresponding idempotent matrices.

Further, by the same assumption, for any $a \in F[G]$, there exists a pseudoinverse $x \equiv \underline{a} \in F[G]$ such that $ax = e_a a x = e_a$. Denote the corresponding matrix $\underline{A} = \mathrm{M}(\underline{a})$, with the property $A\underline{A} = E_A$. Together with $A = E_A A$, this implies

$$\operatorname{rank}(E_A) = \operatorname{rank}(A).$$

Given a binary string $\boldsymbol{\alpha} = (\alpha_1, \alpha_2, \ldots, \alpha_D) \in \mathbb{F}_2^D$, consider the idempotent matrices

$$E_{\boldsymbol{\alpha}} \equiv \prod_{i=1}^{D} E_i^{\alpha_i} (I - E_i)^{1-\alpha_i}.$$

By construction, these commute with all block matrices A, B, …, and satisfy the following orthogonality and completeness properties:

$$E_{\boldsymbol{\alpha}} E_{\boldsymbol{\alpha}'} = I_\ell \delta_{\boldsymbol{\alpha},\boldsymbol{\alpha}'}, \qquad \sum_{\boldsymbol{\alpha} \in \mathbb{F}_2^D} E_{\boldsymbol{\alpha}} = I_\ell. \tag{B1}$$

Consider a boundary operator (matrix) Q_j, $1 \leq j \leq D$ of a known block-size $r \times c$, and the corresponding matrix $Q_j(\boldsymbol{\alpha})$ with each block row multiplied by $E_{\boldsymbol{\alpha}}$. By properties of idempotent matrices $E_{\boldsymbol{\alpha}}$, nonzero rows in $Q_j(\boldsymbol{\alpha})$ with different $\boldsymbol{\alpha}$ are linearly independent. Also, this is an

invertible transformation, thus

$$\operatorname{rank} Q_j = \sum_{\boldsymbol{\alpha}\in\mathbb{F}_2^D} \operatorname{rank} Q_j(\boldsymbol{\alpha}).$$

Now, consider $Q_j(\boldsymbol{\alpha})$ for $\boldsymbol{\alpha} \neq 0$; without limiting generality, assume $\alpha_1 \neq 0$, so that the matrix block $E_{\boldsymbol{\alpha}}A \neq 0$ has the same rank as the corresponding idempotent $E_{\boldsymbol{\alpha}}$. Due to the existence of the pseudoinverse $\underline{A}$, for every other matrix block, e.g., originating from the matrix B, we have

$$E_{\boldsymbol{\alpha}}B = E_{\boldsymbol{\alpha}}E_A A\underline{A}B = (E_{\boldsymbol{\alpha}}A)\,\underline{A}B.$$

Evidently, thus projected blocks contain factors $E_{\boldsymbol{\alpha}}A$ and thus satisfy the conditions of Lemma B1, which gives

$$\operatorname{rank} Q_j(\boldsymbol{\alpha}) = \binom{D-1}{j-1} \operatorname{rank} E_{\boldsymbol{\alpha}}A = \binom{D-1}{j-1} \operatorname{rank} E_{\boldsymbol{\alpha}},$$

where $\alpha_1 \neq 0$. The same construction works with other nonzero $\boldsymbol{\alpha}$, while for $\boldsymbol{\alpha} = \mathbf{0}$ the projected matrix is identically zero, and thus $\operatorname{rank} Q_j(\mathbf{0}) = 0$. This gives, finally, with the help of the completeness relation in Eq. (B1),

$$\begin{aligned}
\operatorname{rank} Q_j &= \sum_{\boldsymbol{\alpha}\in\mathbb{F}_2^D} \operatorname{rank} Q_j(\boldsymbol{\alpha}) \\
&= \sum_{\boldsymbol{\alpha}} (1-\delta_{\mathbf{0},\boldsymbol{\alpha}}) \binom{D-1}{j-1} \operatorname{rank} E_{\boldsymbol{\alpha}} \\
&= \binom{D-1}{j-1} [\operatorname{rank} I_\ell - \operatorname{rank} E_{\mathbf{0}}] \\
&= \binom{D-1}{j-1} (\ell - \kappa), \quad \kappa \equiv \operatorname{rank} E_{\mathbf{0}},
\end{aligned}$$

with κ being the rank of the products of idempotent matrices $(I-E_A)$, $(I-E_B)$, ..., complementary to the commuting blocks $A, B, \ldots$ used to construct the D-complex.

The proof is completed by noticing that for $j = D$, the binomial coefficient equals 1, thus $\operatorname{rank} Q_D = \ell - \kappa$. ■

APPENDIX C: PROOF OF STATEMENT 4

The proof amounts to an observation that the construction gives a D-dimensional QHP code constructed from the F-linear abelian group code with the check matrix $A = \mathrm{M}(a)$. With $k = 0$, all homology groups are trivial, and all distances are infinite. Otherwise, the 1-complex with the boundary operator A has both subspaces of dimensions ℓ, both homology groups of dimensions k, and the homological distances $d_0^{(1)} = 1$, $d_1^{(1)} = d$. This gives the parameters of the product complex: homology group dimensions k_j follow immediately the Künneth formula (11) as the coefficient of x^j in the Poincaré polynomial $(k + xk)^D$, subspace dimensions similarly from Eq. (10) written as a Poincaré polynomial $(\ell + x\ell)^D$, and distances from Theorem 17 in Ref. [21].

APPENDIX D: PROOF OF STATEMENT 5

It is trivial to verify that the Statement is true for $j = 0$ and for $j = D$. Denote $r \equiv m_j^D = \binom{D}{j}$ and $c \equiv m_{j+1}^D = \binom{D}{j+1}$ the block dimensions of subspaces $\mathcal{Q}_j$ and $\mathcal{Q}_{j+1}$, respectively. For any nonzero vector $\boldsymbol{u}$ in $C_h^\perp$, we can construct r same-weight vectors $\boldsymbol{u}_i$ in the space $\mathcal{Q}_j$ (with nonzero elements in only one block, and that equal to $\boldsymbol{u}$) which satisfy the equation $Q_j \boldsymbol{u}_i = \mathbf{0}$. We would like to show that all of them cannot be homologically trivial at the same time.

To this end, define $g(x) = (x^\ell - 1)/h(x)$ and write the nonzero codeword as $u(x) = i(x)g(x)$, with $\deg i(x) < k$, and assume all r vectors $\boldsymbol{u}_i$ to be trivial. The corresponding condition can be written as a matrix-polynomial equation

$$u(x) I_{r\times r} = Q_j(x)\, \Xi_{r\times c}(x) \bmod x^\ell - 1,$$

where $\Xi_{r\times c}(x)$ is a matrix of unknowns of specified dimensions, with elements in the ring $F[x]/(x^\ell - 1)$. With the help of the invertible transformations similar to those constructed in Sec. A, matrix $Q_j(x)$ can be transformed to a diagonal form,

$$Q_j(x) = W_L(x) h(x) \Lambda_{r\times c} W_R(x),$$

with square matrices $W_L(x)$ and $W_R(x)$ invertible in $F[x]/(x^\ell - 1)$, and $\Lambda_{r\times c}$ with only

$$\operatorname{rank} \Lambda_{r\times c} = m_j^{D-1} < \min(r, c)$$

nonzero elements (equal to 1), all in different rows and columns. Using the fact that the object on the left-hand-side (l.h.s.) is proportional to the identity matrix, after a multiplication by $W_L^{-1}(x)$ on the left and $W_L(x)$ on the right, we have

$$\begin{aligned}
u(x) I_{r\times r} &= W_L(x) h(x) \Lambda_{r\times c} W_R(x)\, \Xi_{r\times c}(x) \bmod x^\ell - 1, \\
u(x) I_{r\times r} &= h(x) \Lambda_{r\times c} \Xi'_{r\times c}(x) \bmod x^\ell - 1,
\end{aligned}$$

where the arbitrary unknown coefficients in $\Xi(x)$ have been replaced with the unknown coefficients in $\Xi'(x) \equiv W_R(x)\, \Xi_{r\times c}(x)\, W_L(x)$; this transformation is one-to-one since the transformation matrices are invertible by construction.

If we pick a zero column in $\Lambda_{r\times c}$, the equation reads $u(x) = 0 \bmod x^\ell - 1$, contradicting the initial assumption. Thus, for any nonzero codeword in $C_h^\perp$, there is a nontrivial vector in $H_j(\mathcal{Q})$ of the same weight, which proves the stated upper bound on the distance.

[1] P. W. Shor, in *Proceedings of the 37th Annual Symposium on Foundations of Computer Science*, IEEE (IEEE Computer Society, Los Alamitos, 1996), pp. 56–65.

[2] D. Gottesman, Stabilizer codes and quantum error correction, Ph.D. thesis, Caltech, 1997.

[3] A. Y. Kitaev, Fault-tolerant quantum computation by anyons, Ann. Phys. **303**, 2 (2003).

[4] S. B. Bravyi and A. Y. Kitaev, Quantum codes on a lattice with boundary, arXiv:quant-ph/9811052, unpublished.

[5] E. Dennis, A. Kitaev, A. Landahl, and J. Preskill, Topological quantum memory, J. Math. Phys. **43**, 4452 (2002).

[6] Google Quantum AI, Suppressing quantum errors by scaling a surface code logical qubit, Nature **614**, 676 (2023).

[7] A. Paetznick *et al.*, Demonstration of logical qubits and repeated error correction with better-than-physical error rates, arXiv:2404.02280, unpublished.

[8] D. Bluvstein *et al.*, Logical quantum processor based on reconfigurable atom arrays, Nature **626**, 58 (2024).

[9] R. Acharya *et al.*, Quantum error correction below the surface code threshold, Nature **638**, 920 (2025).

[10] A. Gong, S. Cammerer, and J. M. Renes, Toward low-latency iterative decoding of QLDPC codes under circuit-level noise, arXiv:2403.18901, unpublished.

[11] L. Skoric, D. E. Browne, K. M. Barnes, N. I. Gillespie, and E. T. Campbell, Parallel window decoding enables scalable fault tolerant quantum computation, Nat. Commun. **14**, 7040 (2023).

[12] H. Bombín, Single-shot fault-tolerant quantum error correction, Phys. Rev. X **5**, 031043 (2015).

[13] B. J. Brown, N. H. Nickerson, and D. E. Browne, Fault-tolerant error correction with the gauge color code, Nat. Commun. **7**, 12302 (2016).

[14] E. T. Campbell, A theory of single-shot error correction for adversarial noise, Quantum Sci. Technol. **4**, 025006 (2019).

[15] Y. Fujiwara, Ability of stabilizer quantum error correction to protect itself from its own imperfection, Phys. Rev. A **90**, 062304 (2014).

[16] A. Ashikhmin, C. Y. Lai, and T. A. Brun, in *2014 IEEE International Symposium on Information Theory* (IEEE, New York, NY, USA, 2014), pp. 546–550.

[17] A. Ashikhmin, C. Y. Lai, and T. A. Brun, in *2016 IEEE International Symposium on Information Theory (ISIT), Barcelona, Spain* (IEEE, New York, NY, USA, 2016), pp. 2274–2278.

[18] N. P. Breuckmann and V. Londe, Single-shot decoding of linear rate LDPC quantum codes with high performance, IEEE Trans. Inf. Theory **68**, 272 (2021).

[19] N. P. Breuckmann, K. Duivenvoorden, D. Michels, and B. M. Terhal, Local decoders for the 2D and 4D toric code, Quantum Inf. Comput. **17**, 0181 (2017).

[20] W. Zeng and L. P. Pryadko, Higher-dimensional quantum hypergraph-product codes with finite rates, Phys. Rev. Lett. **122**, 230501 (2019).

[21] W. Zeng and L. P. Pryadko, Minimal distances for certain quantum product codes and tensor products of chain complexes, Phys. Rev. A **102**, 062402 (2020).

[22] A. O. Quintavalle, M. Vasmer, J. Roffe, and E. T. Campbell, Single-shot error correction of three-dimensional homological product codes, PRX Quantum **2**, 020340 (2021).

[23] O. Higgott and N. P. Breuckmann, Improved single-shot decoding of higher-dimensional hypergraph-product codes, PRX Quantum **4**, 020332 (2023).

[24] A. A. Kovalev and L. P. Pryadko, Quantum Kronecker sum-product low-density parity-check codes with finite rate, Phys. Rev. A **88**, 012311 (2013).

[25] H.-K. Lin, X. Liu, P. K. Lim, and L. P. Pryadko, Single-shot and two-shot decoding with generalized bicycle codes, arXiv:2502.19406, unpublished.

[26] R. Wang and L. P. Pryadko, Distance bounds for generalized bicycle codes, Symmetry **14**, 1348 (2022).

[27] R. Wang, H.-K. Lin, and L. P. Pryadko, in *2023 12th International Symposium on Topics in Coding (ISTC), Brest, France* (IEEE, New York, NY, USA, 2023), pp. 1–5.

[28] H.-K. Lin and L. P. Pryadko, Quantum two-block group algebra codes, Phys. Rev. A **109**, 022407 (2024).

[29] S. Bravyi, A. W. Cross, J. M. Gambetta, D. Maslov, P. Rall, and T. J. Yoder, High-threshold and low-overhead fault-tolerant quantum memory, Nature **627**, 778 (2024).

[30] Z. Liang, K. Liu, H. Song, and Y.-A. Chen, Generalized toric codes on twisted tori for quantum error correction, PRX Quantum **6**, 020357 (2025).

[31] N. Berthusen, D. Devulapalli, E. Schoute, A. M. Childs, M. J. Gullans, A. V. Gorshkov, and D. Gottesman, Toward a 2D local implementation of quantum low-density parity-check codes, PRX Quantum **6**, 010306 (2025).

[32] K. Wang *et al.*, Demonstration of low-overhead quantum error correction codes, Nat. Phys. **22**, 308 (2026).

[33] D. Aasen, J. Haah, M. B. Hastings, and Z. Wang, Geometrically enhanced topological quantum codes, arXiv:2505.10403, unpublished.

[34] D. Aasen, M. B. Hastings, V. Kliuchnikov, J. M. Bello-Rivas, A. Paetznick, R. Chao, B. W. Reichardt, M. Zanner, M. P. da Silva, Z. Wang, and K. M. Svore, A topologically fault-tolerant quantum computer with four dimensional geometric codes, arXiv:2506.15130, unpublished.

[35] J.-P. Tillich and G. Zémor, in *Proc. IEEE Int. Symp. Inf. Theory (ISIT)* (2009), pp. 799–803.

[36] M. Borello, J. De La Cruz, and W. Willems, On checkable codes in group algebras, J. Algebra Appl. **21**, 2250125 (2022).

[37] A. R. Calderbank and P. W. Shor, Good quantum error-correcting codes exist, Phys. Rev. A **54**, 1098 (1996).

[38] A. M. Steane, Simple quantum error-correcting codes, Phys. Rev. A **54**, 4741 (1996).

[39] Commuting matrices can be constructed for any pair of group algebra elements even for a non-abelian group [66]. While there is no direct generalization for arbitrary sets of $D > 2$ non-abelian group algebra elements, less general constructions do exist. These go outside the scope of the present work.

[40] Such a decomposition exists according to the Fundamental Theorem of finite abelian groups.

[41] Otherwise, the spaces in an AMC complex can be decomposed onto a direct sum of subspaces corresponding to cosets of the subgroup $G_X = \langle\{x_j\}\rangle$ in the original group G; see Sec. IV C in Ref. [28]. In the abelian case these complexes are permutation-equivalent to a complex in the subgroup $G_X \leq G$.

[42] Note, however, that the circuit distance need not always coincide with that of the original code. As an example, while any single-ancilla measurement circuit would work for a toric code [67], rotated surface codes require

a carefully designed N-Z addressing scheme for fault-tolerance [53].

[43] J. J. Postema and S. J. J. M. F. Kokkelmans, Existence and characterisation of bivariate bicycle codes, arXiv:2502.17052, unpublished.

[44] P. Panteleev and G. Kalachev, Degenerate quantum LDPC codes with good finite length performance, Quantum **5**, 585 (2021).

[45] Y. A. Drozd and V. V. Kirichenko, *Finite Dimensional Algebras* (Springer-Verlag, Berlin, Heidelberg, 1994).

[46] P. Panteleev and G. Kalachev, Quantum LDPC codes with almost linear minimum distance, IEEE Trans. Inf. Theory **68**, 213 (2022).

[47] Y. Fan and L. Lin, Dihedral group codes over finite fields, IEEE Trans. Inf. Theory **67**, 5016 (2021).

[48] L. M. Bazzi and S. K. Mitter, Some randomized code constructions from group actions, IEEE Trans. Inf. Theory **52**, 3210 (2006).

[49] I. Haviv, M. Langberg, M. Schwartz, and E. Yaakobi, in *2017 IEEE International Symposium on Information Theory (ISIT), Aachen, Germany* (IEEE, New York, NY, USA, 2017), pp. 586–588.

[50] S. Lin and E. J. Weldon, Long BCH codes are bad, Inf. Control **11**, 445 (1967).

[51] E. Berlekamp and J. Justesen, Some long cyclic linear binary codes are not so bad, IEEE Trans. Inf. Theory **20**, 351 (1974).

[52] L. P. Pryadko and W. Zeng, dist-m4ri—Distance of a classical or quantum CSS code, 2024, https://github.com/QEC-pages/dist-m4ri.

[53] Y. Tomita and K. M. Svore, Low-distance surface codes under realistic quantum noise, Phys. Rev. A **90**, 062320 (2014).

[54] To guarantee rank preservation after removal of a block row (which is important for the 1111 cycle), guided by Lemma B1, the polynomials were ordered so that $a_4 = 1 + x$ [which gives block D in Eqs. (27) and (28)].

[55] C. Gidney, Stim: A fast stabilizer circuit simulator, Quantum **5**, 497 (2021).

[56] L. P. Pryadko, vecdec—Vectorized decoder and LER estimator, 2025, https://github.com/QEC-pages/vecdec.

[57] I. Dumer, A. A. Kovalev, and L. P. Pryadko, Distance verification for classical and quantum LDPC codes, IEEE Trans. Inf. Theory **63**, 4675 (2017).

[58] This is unlike with the BP+OSD package [68,69] whose performance may actually be degraded by additional detector events, see in Appendix A of Ref. [70]. In comparison, for the decoder used here, removing minority detector events increases logical error rates, e.g., from 0.20% to 0.36% at $p = 0.1\%$ with the [[42, 6, 4]] code and the "1212" circuits.

[59] A. Grospellier, L. Grouès, A. Krishna, and A. Leverrier, Combining hard and soft decoders for hypergraph product codes, Quantum **5**, 432 (2021).

[60] A. A. Kovalev and L. P. Pryadko, Fault tolerance of quantum low-density parity check codes with sublinear distance scaling, Phys. Rev. A **87**, 020304(R) (2013).

[61] I. Dumer, A. A. Kovalev, and L. P. Pryadko, Thresholds for correcting errors, erasures, and faulty syndrome measurements in degenerate quantum codes, Phys. Rev. Lett. **115**, 050502 (2015).

[62] A. M. Stephens, Fault-tolerant thresholds for quantum error correction with the surface code, Phys. Rev. A **89**, 022321 (2014).

[63] P. Das, A. Locharla, and C. Jones, LILLIPUT: A lightweight low-latency lookup-table based decoder for near-term quantum error, in *Proceedings of 27th ACM ASPLOS* (ACM, New York, NY, USA, 2022), pp. 541.

[64] H. Bombin, R. W. Chhajlany, M. Horodecki, and M. A. Martin-Delgado, Self-correcting quantum computers, New J. Phys. **15**, 055023 (2013).

[65] M. B. Hastings, Decoding in hyperbolic spaces: LDPC codes with linear rate and efficient error correction, Quantum Inf. Comput. **14**, 1187 (2014).

[66] P. Panteleev and G. Kalachev, Asymptotically good quantum and locally testable classical LDPC codes, in *Proceedings of the 54th Annual ACM SIGACT Symposium on Theory of Computing* (ACM, New York, NY, USA, 2022), pp. 375–388.

[67] A. G. Manes and J. Claes, Distance-preserving stabilizer measurements in hypergraph product codes, Quantum **9**, 1618 (2025).

[68] J. Roffe, D. R. White, S. Burton, and E. Campbell, Decoding across the quantum low-density parity-check code landscape, Phys. Rev. Res. **2**, 043423 (2020).

[69] J. Roffe, LDPC: Python tools for low density parity check codes, PyPi repository, 2022, https://pypi.org/project/ldpc/.

[70] L. A. Beni, O. Higgott, and N. Shutty, Tesseract: A search-based decoder for quantum error correction, arXiv:2503.10988, unpublished.